

Gísli Björn Helgason
July 1, 2022
Master thesis defence

Downscaling wind fields using deep learning

Outline

- Motivation and background
- Data and methods
- Results
- Conclusions and future work

Motivation

- Refinement of globally simulated wind data (ERA5)
 - More accurate assessment
- Dynamical downscaling (WRF) still computationally demanding
- Deep learning as WRF model surrogate
 - Learning from dynamically downscaled data

Super resolution

- Enhancement of images
- Similar to downscaling of atmospheric fields
- Deep learning very successful

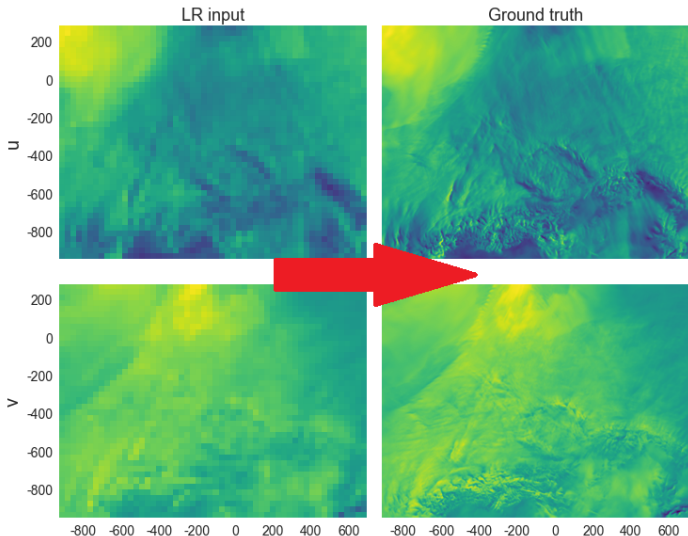


Figure 1: SR example

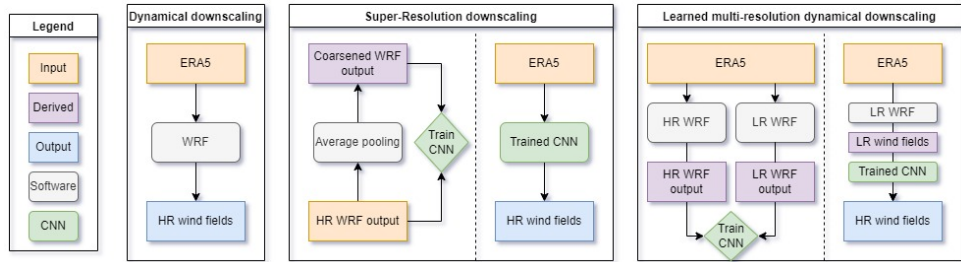


Figure 2: Dynamical and SR downscaling framework

Convolutional Neural Networks (CNNs)

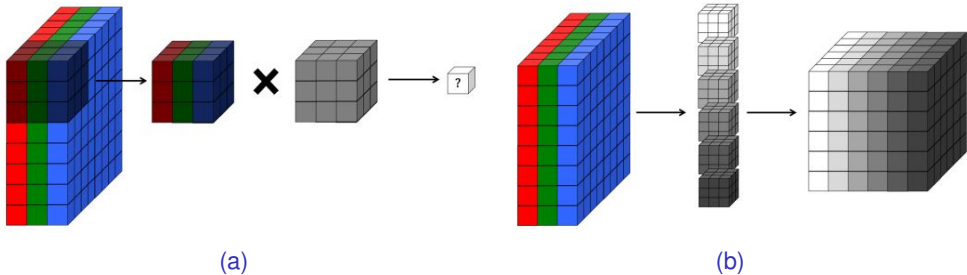


Figure 3: (a) Application of a volumetric 2D convolutional filter to a full-color RGB image and (b) a 3D visualization of a convolutional layer (Buduma and Locascio, 2017).

Convolutional Neural Networks (CNNs)

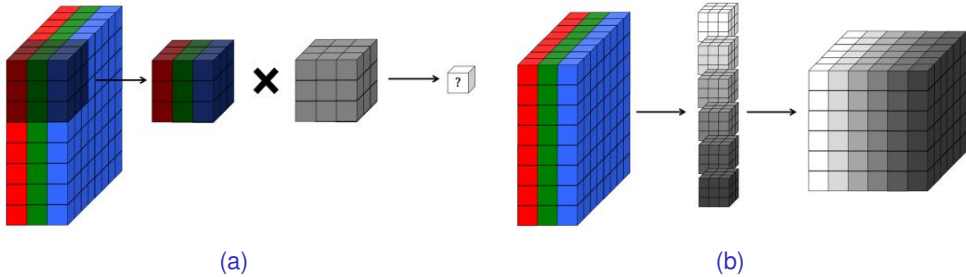


Figure 3: (a) Application of a volumetric 2D convolutional filter to a full-color RGB image and (b) a 3D visualization of a convolutional layer (Buduma and Locascio, 2017).

$$m_{ij} = f((\mathbf{w} * \mathbf{x})_{ij} + b)$$

Conditional Generative Adversarial Networks (GANs)

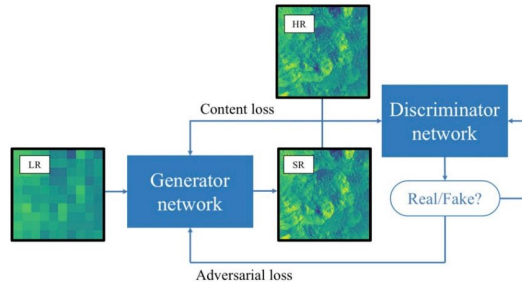


Figure 4: Schematic of SRGAN (Stengel et al., 2020)

Conditional Generative Adversarial Networks (GANs)

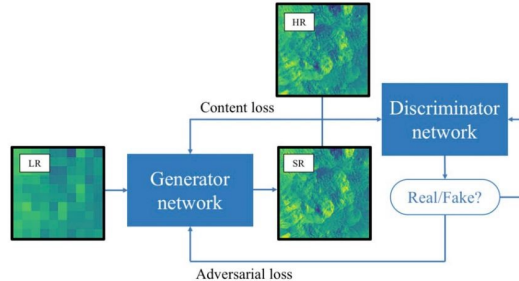


Figure 4: Schematic of SRGAN (Stengel et al., 2020)

- Wasserstein GAN with Gradient Penalty (Gulrajani et al., 2017)

$$L_D(x, t) = E[D(G(x))] - E[D(t)] + GP(x, t) \quad (1)$$

$$L_G(x, t) = -E[D(G(x))] + L_c(x, t) \quad (2)$$

Deep learning based wind field downscaling

- Höhlein et al. (2020) compared several SRCNN architectures
 - Regressing on topographic data significantly improves the performance
 - CNNs are more flexible than multinomial regression

Deep learning based wind field downscaling

- Höhlein et al. (2020) compared several SRCNN architectures
 - Regressing on topographic data significantly improves the performance
 - CNNs are more flexible than multinomial regression
- Stengel et al. (2020) SRGAN
 - 50x SR of climate fields (idealized pairings)
 - GANs give more realistic output
 - Unstable training

This work

- Further quantify how and if HR topographical data can be used to improve the reconstruction ability and spatial generalisability
- Investigate the nature of high-frequency features resulting from adversarial training

This work

“Can deep learning be considered a reliable technique for mesoscale wind field downscaling in the purpose of wind resource assessment?”

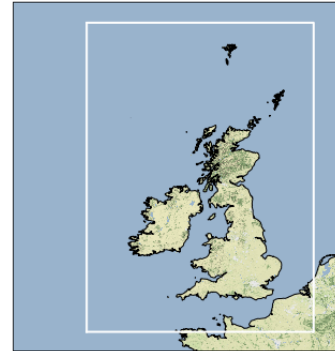
Data

- Post-processed 100 m wind fields from NEWA database
 - 2007-2010 test (CE and GB domains)
 - 2011-2016 train (CE domain)
 - 2017,2018 validation during training
 - Sampled every 3h
- HR topographic data
 - LSM and HGT

NEWA domains



(a)



(b)

Figure 5: (a) The Central Europe (CE) and (b) the Great Britain (GB) NEWA model domains.

Methods

- Models
 - CNN
 - WGAN
 - Bicubic baseline
- Networks trained using GPU
 - HPC UOL
 - NVIDIA Tesla GPUs with 16GB memory
- Patch training

Training and test framework

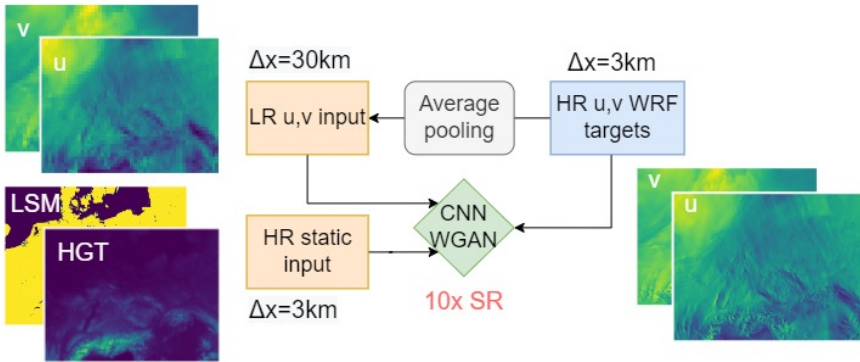
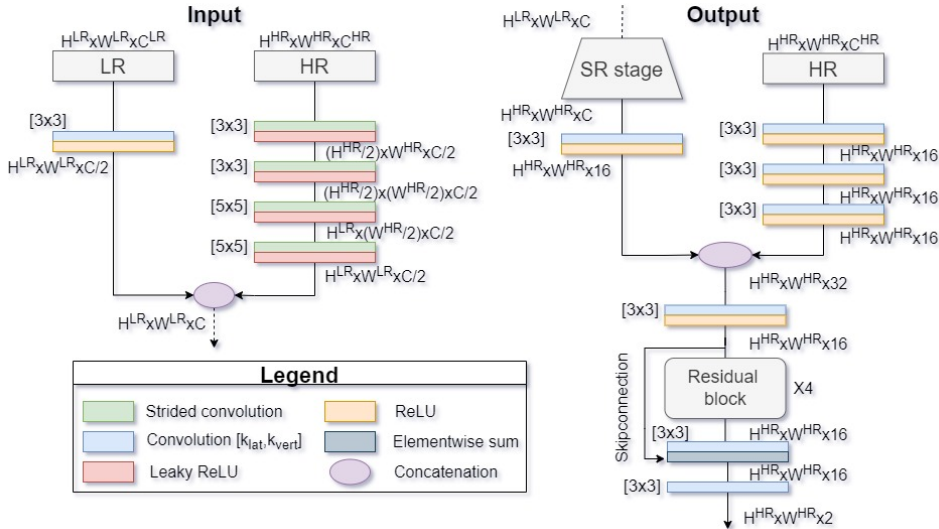


Figure 6: Illustration of the training approach and data fields.

Generator network extension to ingest HR static data



Generator network ablation study

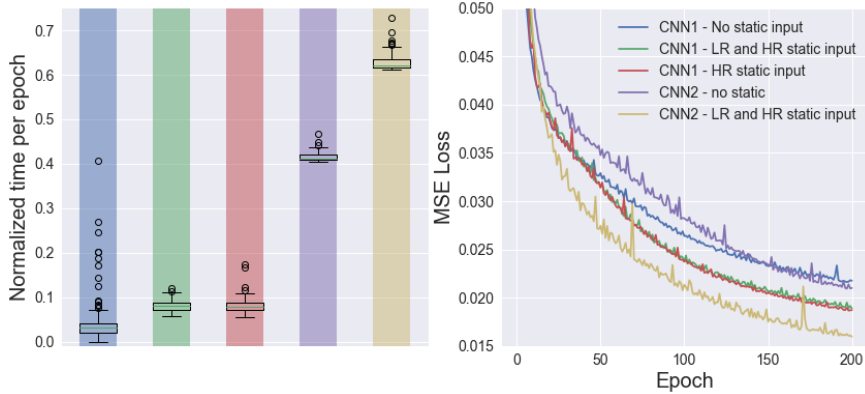


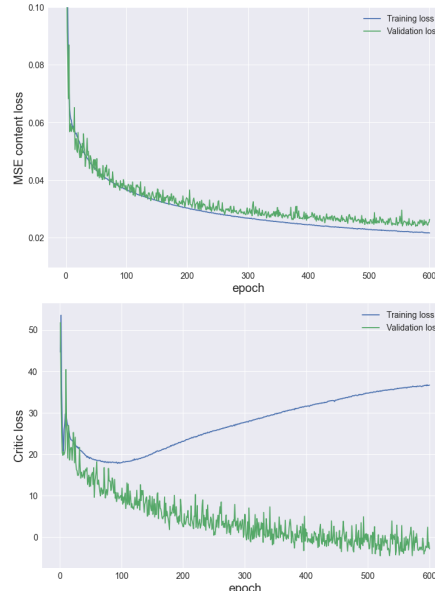
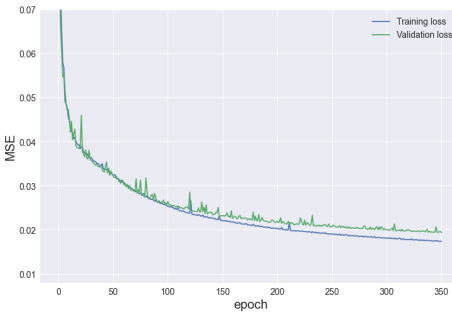
Figure 8: Statistics of normalized time per epoch during training and the evolution of MSE loss on the standardized training set.

Evaluation metrics

- $\text{MSE} = \left\langle \left\| \vec{t} - \vec{y} \right\|^2 \right\rangle_{Dom}$
- $\text{CosDis} = \frac{1}{2} \left(1 - \left\langle \cos \left(\vec{t}_i, \vec{y}_i \right) \right\rangle \right) = \frac{1}{2} \left(1 - \left\langle \frac{\vec{t}_i \cdot \vec{y}_i}{\|\vec{t}_i\| \|\vec{y}_i\|} \right\rangle \right)$
- $\text{MD} = \left\langle \|\vec{t}_i\| - \|\vec{y}_i\| \right\rangle$
- $S(k) = \frac{\Delta x}{2\pi N} |X(k)|^2$

Results

- Training time
 - ~ 5 days for GAN
 - ~ 2 days for CNN
- Deployment in matter of minutes!



Test set results

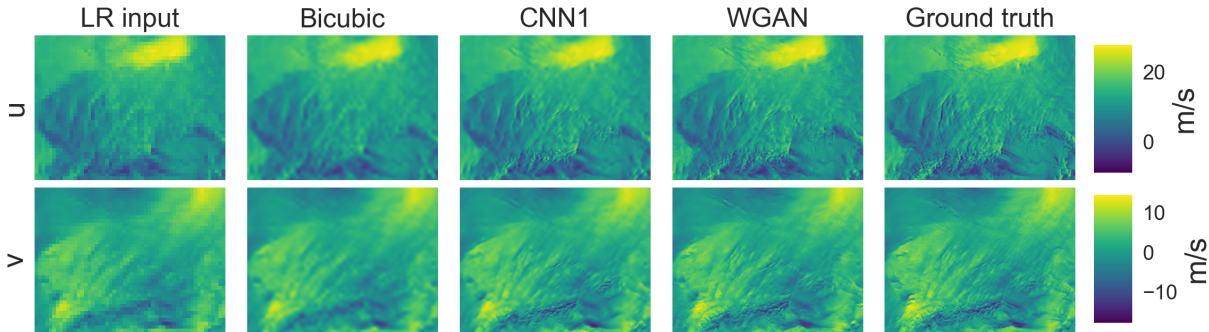


Figure 10: Comparison of various SR methods on NEWA CE domain data fields.

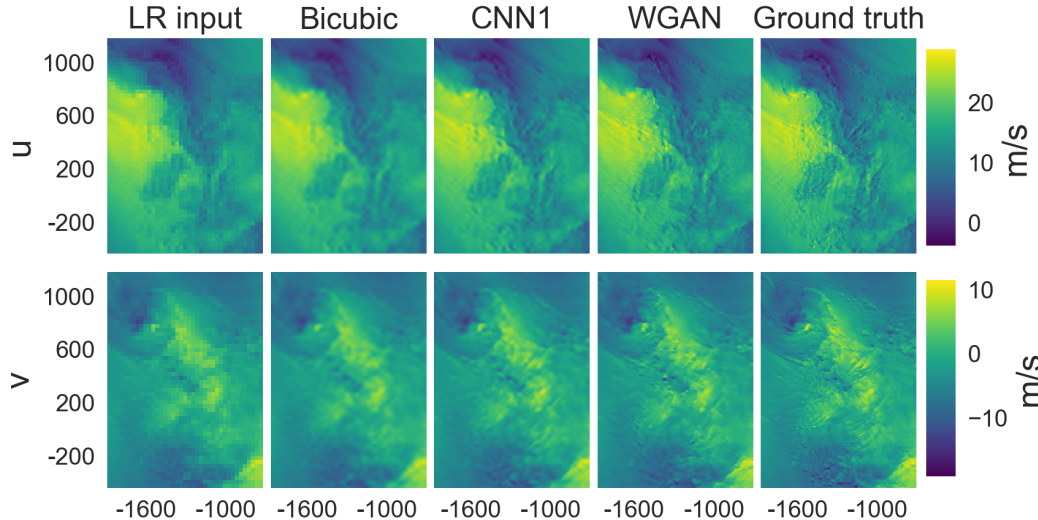


Figure 11: Comparison of various SR methods on NEWA GB domain data fields.

Domain averaged MSE

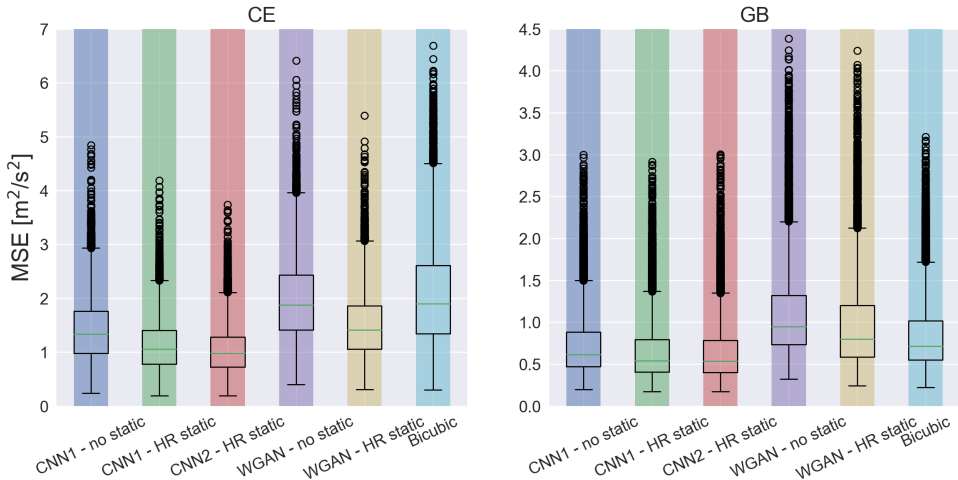


Figure 12: Statistics of spatially averaged MSE on the test set

Spatial distribution of systematic reconstruction errors

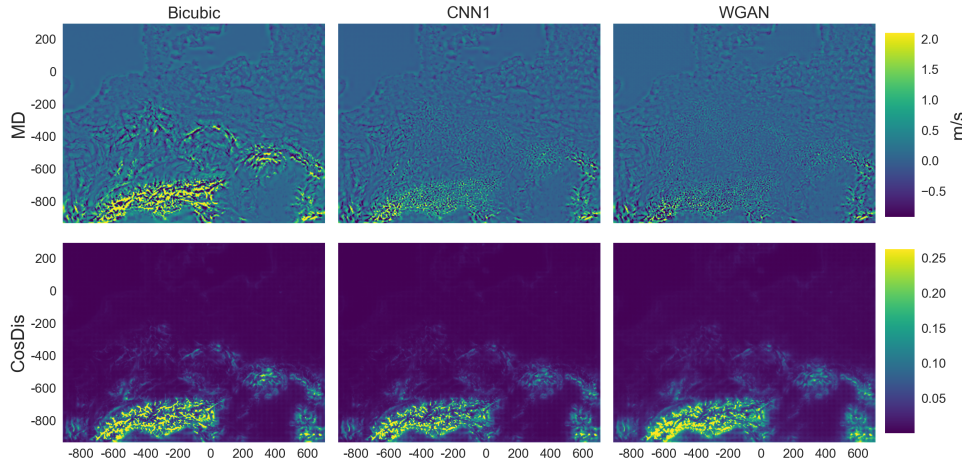


Figure 13: Mean magnitude difference (top row) and mean cosine deviations (bottom row) on the CE domain

Spatial distribution of systematic reconstruction errors

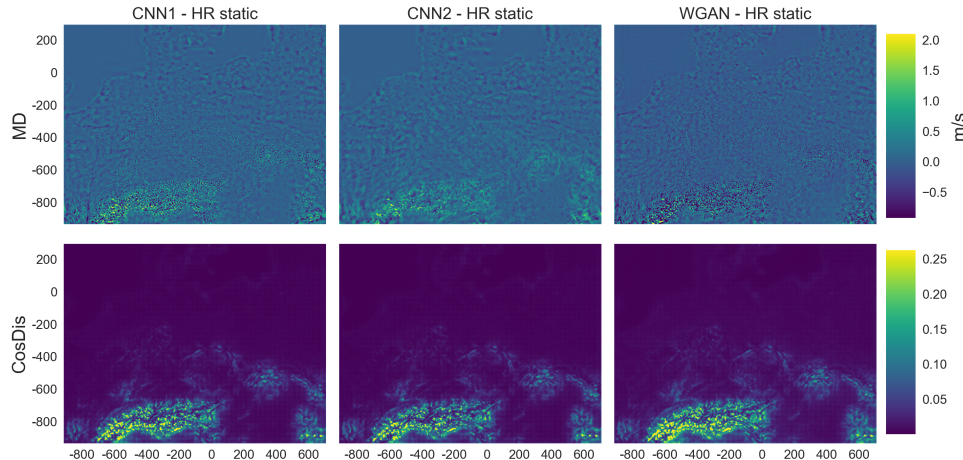


Figure 14: Mean magnitude difference (top row) and mean cosine deviations (bottom row) on the CE domain

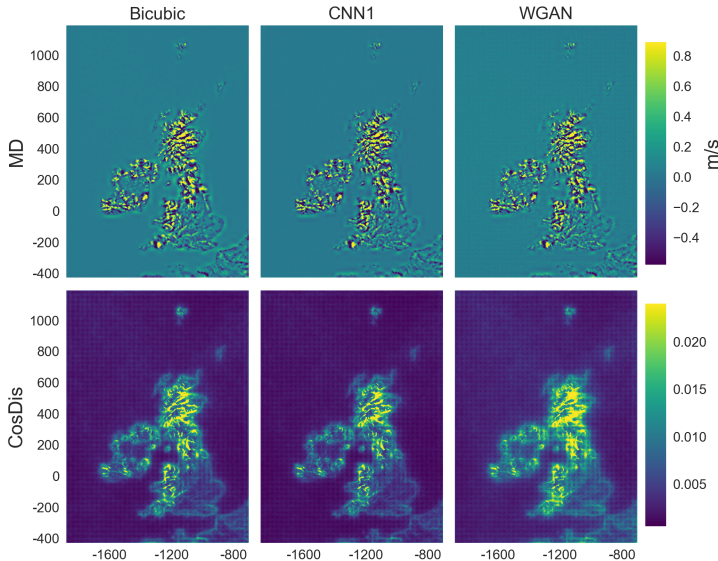


Figure 15: Mean magnitude difference (top row) and mean cosine deviations (bottom row) on the GB domain

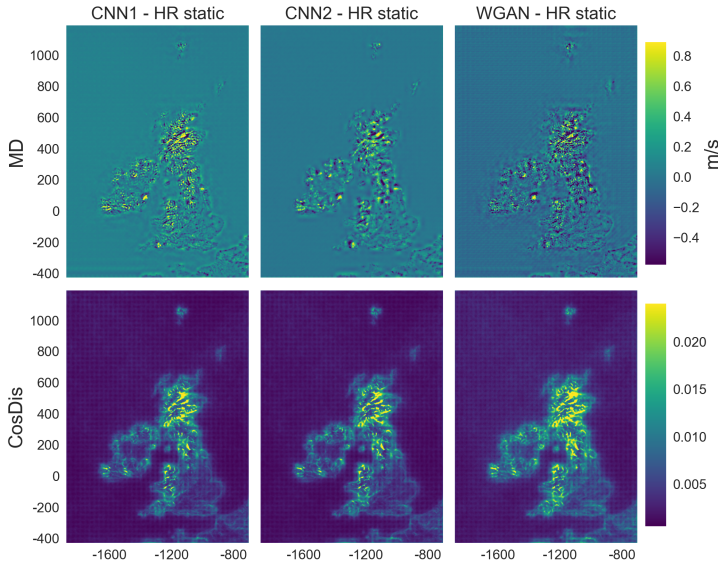
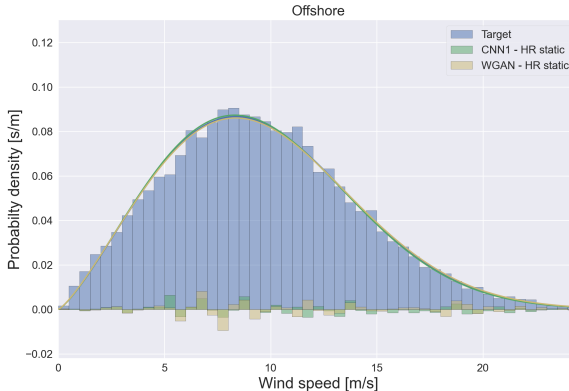


Figure 16: Mean magnitude difference (top row) and mean cosine deviations (bottom row) on the GB domain

Long term distributions and Weibull fitting



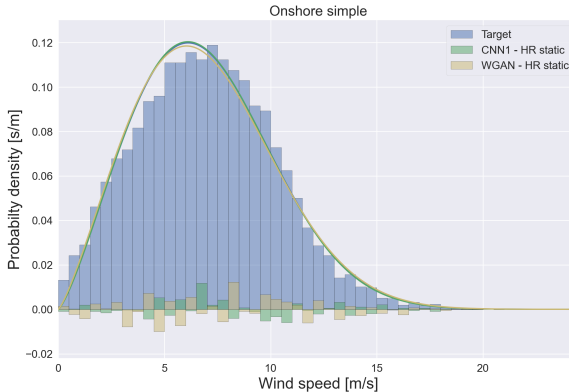
(a)



(b)

Figure 17: (a) Target probability density and model output difference along with Weibull fits. (b) Site location.

Long term distributions and Weibull fitting



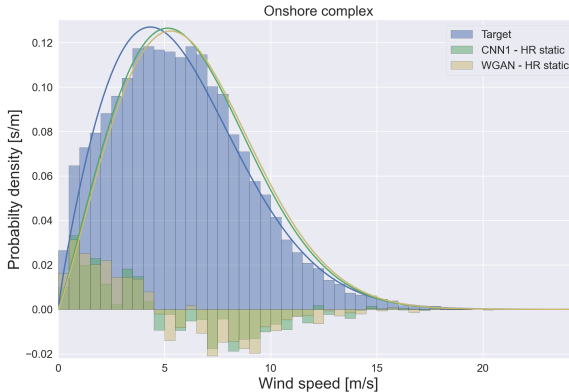
(a)



(b)

Figure 17: (a) Target probability density and model output difference along with Weibull fits. (b) Site location.

Long term distributions and Weibull fitting



(a)



(b)

Figure 17: (a) Target probability density and model output difference along with Weibull fits. (b) Site location.

Long term distributions and Weibull fitting

Table 1: Fitted values and relative difference between target and model output.

Site	Parameter	Target	CNN1	WGAN
			HR static	HR static
Onshore Complex	μ [m/s]	5.8	6.2	6.3
	k	1.9	2.1	2.1
	A [m/s]	6.5	7.0	7.1
	$\Delta\mu$ [%]	-	7.6	9.6
	Δk [%]	-	11.7	13.0
	ΔA [%]	-	7.9	9.9

Spectral analysis

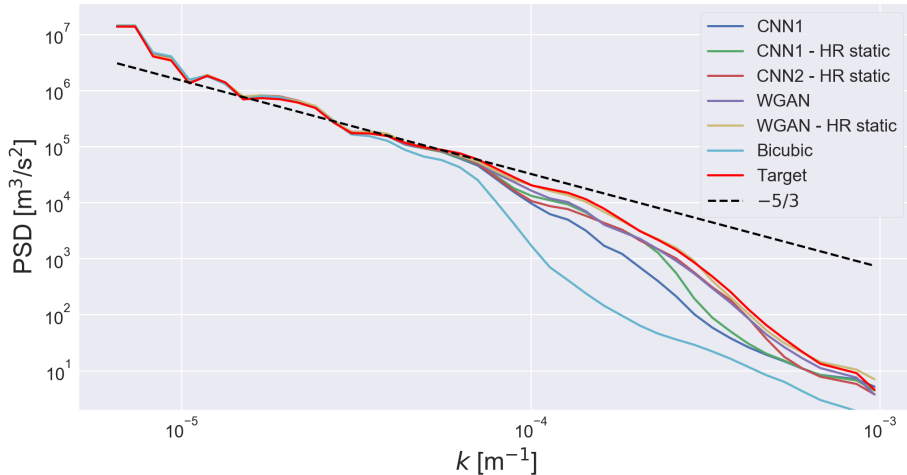


Figure 17: Radially averaged 2D spectrum

Take home messages

- Topographically aware CNNs and GANs can accurately reproduce wind speed climatologies

Take home messages

- Topographically aware CNNs and GANs can accurately reproduce wind speed climatologies
- Leveraging HR static data improves performance in complex terrain
 - Reduces systematic underpredictions in wind speed magnitude

Take home messages

- Topographically aware CNNs and GANs can accurately reproduce wind speed climatologies
- Leveraging HR static data improves performance in complex terrain
 - Reduces systematic underpredictions in wind speed magnitude
- GANs yield more fine scale variability
 - Enhances directional deviations in complex terrain

Future work

- Involve more NEWA domains in model training
- Model temporal evolution of wind fields (Video-SR)
 - Recurrent neural networks

Future work

- Involve more NEWA domains in model training
- Model temporal evolution of wind fields (Video-SR)
 - Recurrent neural networks
- Explore ways to make the SR framework more realistic
 - Graph based networks to address grid mismatch
 - Train networks using WRF parent domain as LR input

Future work

- Involve more NEWA domains in model training
- Model temporal evolution of wind fields (Video-SR)
 - Recurrent neural networks
- Explore ways to make the SR framework more realistic
 - Graph based networks to address grid mismatch
 - Train networks using WRF parent domain as LR input
- Further develop ensemble based probabilistic SR
 - Assess uncertainty quantification via rank statistics

Ensemble based SR

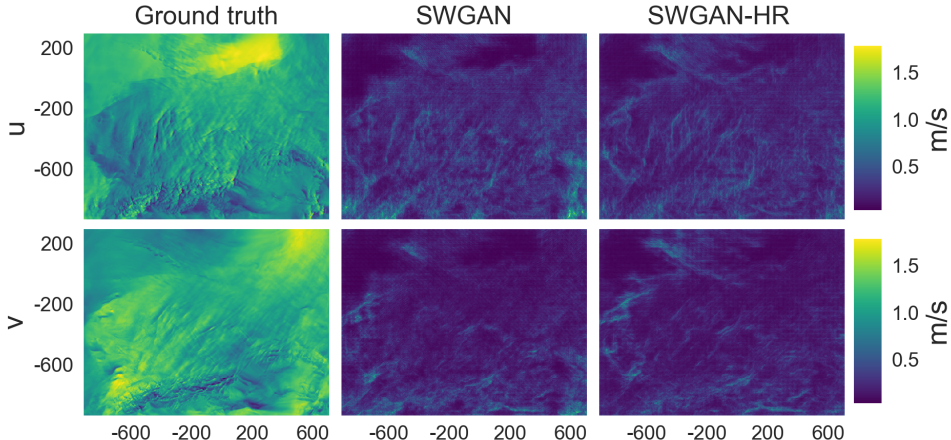


Figure 18: Ensemble standard deviation of 100 images generated by the stochastic WGAN models with and without HR static data.

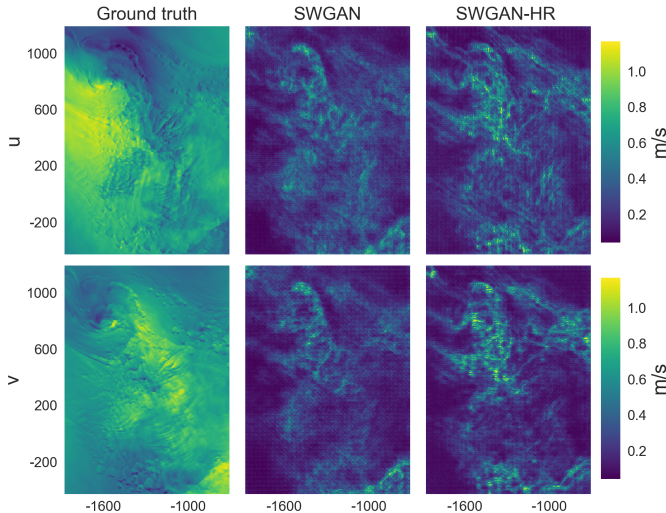


Figure 19: Ensemble standard deviation of 100 images generated by the stochastic WGAN models with and without HR static data.

References I

-  Buduma, Nikhil and Nicholas Locascio (2017). *Fundamentals of Deep Learning: Designing Next-Generation Machine Intelligence Algorithms*. 1st. O'Reilly Media, Inc. ISBN: 1491925612.
-  Stengel, Karen et al. (July 2020). "Adversarial super-resolution of climatological wind and solar data". In: *Proceedings of the National Academy of Sciences* 117.29, pp. 16805–16815. ISSN: 0027-8424. DOI: 10.1073/PNAS.1918964117. URL: <https://www.pnas.org/content/117/29/16805>.
-  Gulrajani, Ishaan et al. (2017). *Improved Training of Wasserstein GANs*. DOI: 10.48550/ARXIV.1704.00028. URL: <https://arxiv.org/abs/1704.00028>.

References II

-  Höhlein, Kevin et al. (Nov. 2020). “A comparative study of convolutional neural network models for wind field downscaling”. In: *Meteorological Applications* 27.6, e1961. ISSN: 1469-8080. DOI: 10.1002/MET.1961. URL: <https://onlinelibrary.wiley.com/doi/full/10.1002/met.1961>.
-  Ledig, Christian et al. (2017). *Photo-Realistic Single Image Super-Resolution Using a Generative Adversarial Network*.

Supporting Material

$$\text{CosDis} = \frac{1}{2} \left(1 - \left\langle \cos \left(\vec{t}_i, \vec{y}_i \right) \right\rangle \right) = \frac{1}{2} \left(1 - \left\langle \frac{\vec{t}_i \cdot \vec{y}_i}{\| \vec{t}_i \| \| \vec{y}_i \|} \right\rangle \right) \quad (3)$$

$$MD = \left\langle \| \vec{t}_i \| - \| \vec{y}_i \| \right\rangle \quad (4)$$

$$\mu_n = A^n \Gamma \left(1 + \frac{n}{k} \right) \quad (5)$$

$$\Gamma(x) = \int_0^{\infty} s^{x-1} \exp(-s) ds. \quad (6)$$

$$\frac{\mu_3}{\mu^3} = \frac{\overline{u^3}}{\bar{u}^3} = \frac{\Gamma(1+3/k)}{\Gamma(1+1/k)}$$

Supporting Material (WGAN-GP)

$$L_D = D(y) - D(t) + \lambda(\|\partial_{\hat{y}} D(\hat{y})\| - 1)^2 \quad (7)$$

$$y = G(x), \quad \hat{y} = \epsilon t + (1 - \epsilon)y \quad (8)$$

$$L_G = L_{content} + \beta L_{adversarial} \quad (9)$$

$$L_{adversarial} = -D(y) \quad (10)$$

$$L_{content} = \left\langle \|t - y\|^2 \right\rangle \quad (11)$$

Original SRGAN architecture

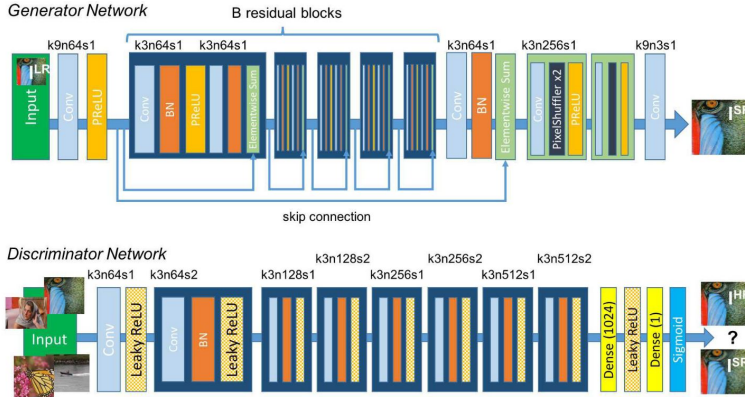


Figure 20: Architecture of the original Generator and Discriminator network with corresponding kernel size (k), number of feature maps (n) and stride (s) indicated for each convolutional layer. Taken from Ledig et al. (2017).

WGAN examples

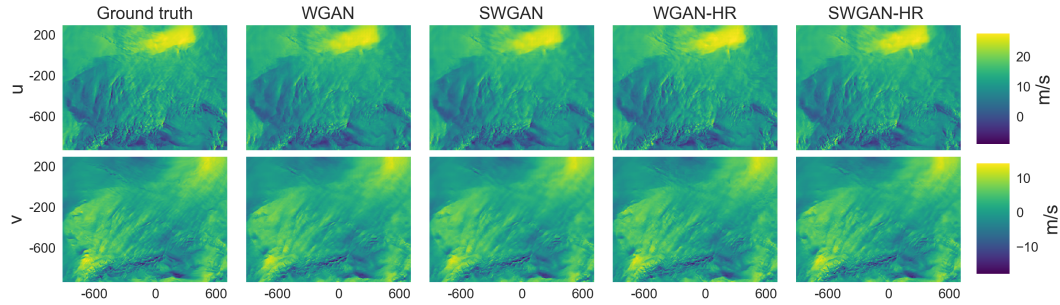


Figure 21: Comparison of WGAN model output and test target from the CE domain.

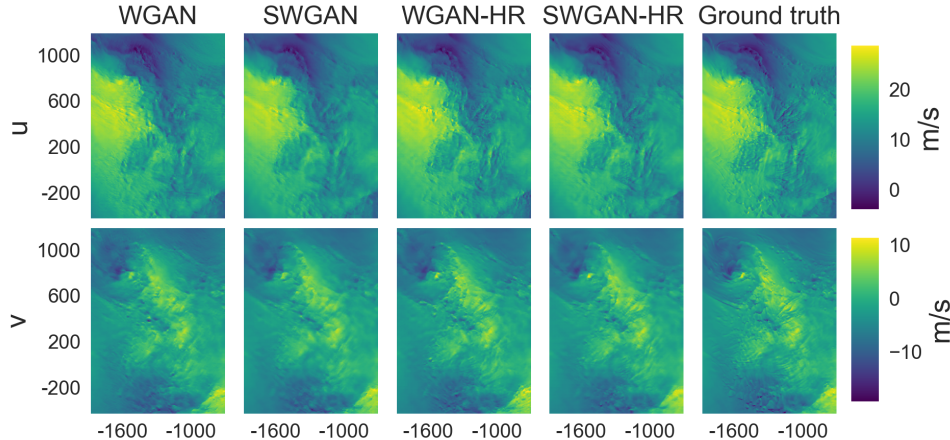


Figure 22: Comparison of WGAN model output and test target from the GB domain.

Test set climatologies

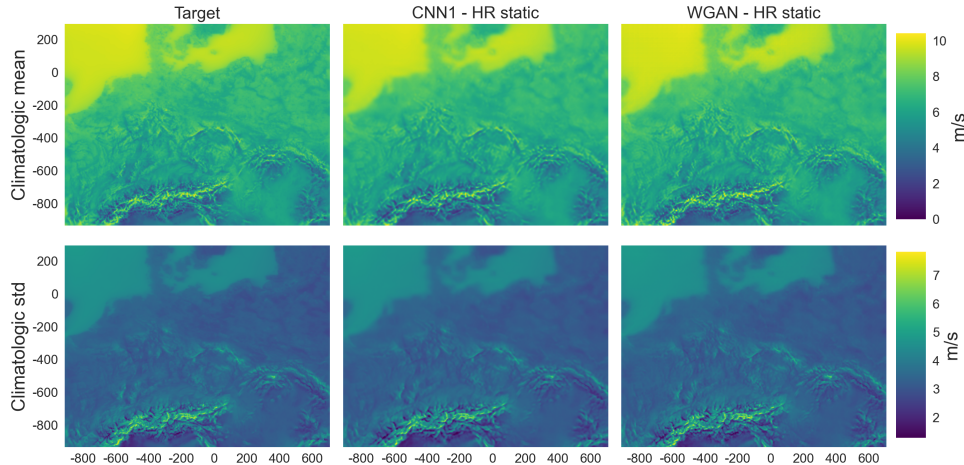


Figure 23: Climatological mean and standard deviation of wind magnitude from the CE test set.

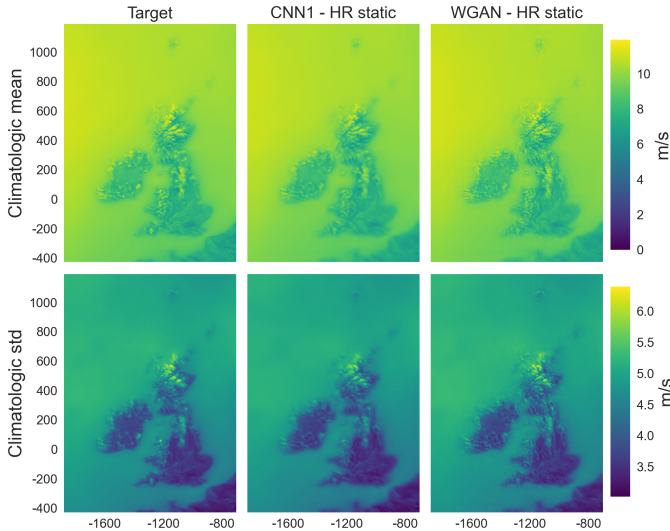
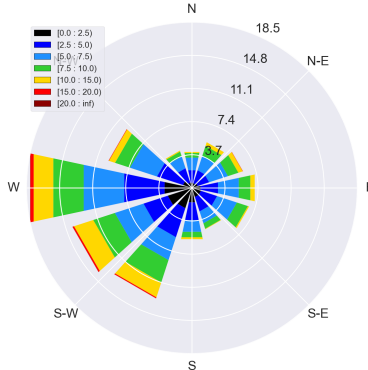
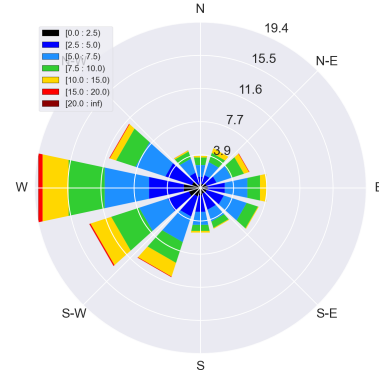


Figure 24: Climatological mean and standard deviation of wind magnitude from the GB test set.

Wind rose at complex site



(a) Target



(b) WGAN - HR static

Figure 25: Wind rose from target and WGAN model output data for the topographically complex site considered in this study.